

Solvothermal Synthesis of Anatase TiO₂ Nanosheets with Exposed {001} Facets (Sintesis Solvoterma Anatase Helaian Nano TiO₂ dengan Faset {001} Terdedah)

MADIHA YASIR, M., TAZLI AZIZAN*, ANITA RAMLI & MARIAM AMEEN

ABSTRACT

Enhancing the catalytic activity of titania (TiO₂) nanomaterials by controlling the size, surface area and percentage of highly reactive exposed {001} facets has become attractive in the recent years because of its wider applications in the different fields of scientific research. In the present study, anatase TiO₂ nano-sized sheets (TNS) were synthesized using a simple ethanol assisted solvothermal chemical route. The TNS structures were characterized using Field Emission Scanning Electron Microscopy (FE-SEM), Transmission electron microscopic (TEM), Raman analysis, X-ray diffraction (XRD) and Accelerated surface area and porosimetry (ASAP) analysis. The results from TEM, Raman and XRD analysis confirmed the presence of anatase crystalline structure of TNS with the size range of 20-40 nm. The synthesized TNS structures possess 60% of highly reactive exposed {001} facets with a total surface area of 73 m²/g. These tremendous crystalline properties of solvothermally synthesized TNS structure makes it as an attractive catalyst for environmental and bio-fuel applications.

Keywords: Anatase TiO₂; nanosheets; solvothermal; {001} Facets

ABSTRAK

Peningkatan aktiviti perangsang menggunakan bahan nano titania (TiO₂) dengan mengawal saiz, permukaan dan peratusan faset {001} terdedah sangat reaktif telah menjadi tarikan dalam beberapa tahun kebelakangan kerana penggunaan yang lebih meluas dalam perbezaan bidang penyelidikan saintifik. Dalam kajian ini, helaian bersaiz nano anatase TiO₂ (TNS) telah disintesis menggunakan laluan etanol mudah berbantu kimia solvoterma. Struktur TNS telah dicirikan menggunakan pancaran medan imbasan elektron mikroskopi (FE-SEM), elektron penghantaran mikroskopik (TEM), analisis Raman, pembelauan sinar-x (XRD) dan kawasan permukaan pecutan serta analisis porosimetri (ASAP). Keputusan daripada analisis TEM, Raman dan XRD mengesahkan kewujudan struktur hablur anatase TNS dengan pelbagai julat saiz 20-40 nm. Struktur sintesis TNS memiliki 60% daripada faset {001} terdedah sangat reaktif dengan jumlah keluasan permukaan 73 m²/g. Sifat kristal solvoterma yang hebat daripada struktur TNS yang disintesis menjadikannya sebagai pemangkin menarik untuk alam sekitar dan aplikasi bio-bahan api.

Kata kunci: Anatase TiO₂; faset {001}; helaian nano; solvoterma

INTRODUCTION

TiO₂ is gaining much more recognition day-by-day due to its wider applications in the fields of photo-catalysis, heterogeneous catalysis, photo-splitting of water and solar cells. The main reasons for the widespread applications of TiO₂ are its chemical and biological inertness, cost effectiveness, strong oxidative as well as corrosive stability. Among other crystalline phases of TiO₂ (rutile and brookite), anatase phase is considered to be the most important, as the size and shape of anatase crystals considerably effect the performance (Dozzi & Selli 2013; Gu et al. 2012).

It has been proved both theoretically and experimentally that different crystal facets of anatase TiO₂ have different degree of reactivity. {001} facet of anatase crystal has been proven to be more reactive than the more abundant {101} facet (Biyoghe Bi Ndong et al. 2014). The reason for low reactivity of {101} facet is associated to their lesser degree of reduction

and low density of surface under-coordinated Ti atoms as compared to {001} facets (Cai et al. 2014). On the other hand, the less abundant {001} facets possess high catalytic reactivity that is almost twofold as compared to {101} crystal facets, which is actually due to presence of high number of under-coordinated Ti atoms and strained atomic configuration at the crystal surface. Moreover, longer Ti-O-Ti bonds indicates highly destabilized and reactive 2p states of surface oxygen atoms which are responsible for higher adsorption of reactant molecules on the surface and as a result show higher reactivity (Cao et al. 2014; Dozzi & Selli 2013; Madiha Yasir 2014; Shi et al. 2014). Along with reactive facets, crystalline size is also important to determine the catalytic activity, as smaller size (usually < 50 nm) is responsible for higher surface area and greater number of active sites (Deng et al. 2014; Xinwen & Zongjian 2013). Therefore, the size of TiO₂ crystals is one of the governing factor to control the catalytic performance of TiO₂ catalysts.

Many efforts have been made in the recent years to control the shape as well as the size of the crystalline species to increase the percentage of reactive crystal facets (Chang et al. 2015; Xiaowei et al. 2015; Yifan et al. 2015). As a result, an improved interaction between the reactants and the surface can be attained, which resulted in higher catalytic activity. Usually, the growth of the crystalline species involves a quick disappearance of high energy facets {001} and an evolution of exposed facets {101} with lower surface free energy, under equilibrium conditions (Chao et al. 2014; Chen et al. 2014). Therefore, the production of exposed high free energy facets is very challenging. In this context, high temperature and the presence of suitable capping agents may be very helpful in order to create non-equilibrium conditions, which are suitable for the growth of high energy facets. Unfortunately, high temperature has not been proven to be desirable as it favours the formation of less reactive rutile phase (Liu et al. 2011). Moreover, capping agents, help to induce the growth of reactive facets anisotropically.

Recently, several studies have been carried out to prepare the anatase TiO₂ crystals with higher percentage of reactive facets {001}, more commonly using hydrofluoric acid (HF) as capping agent. Yang et al. (2009) prepared titania nanosheets using titanium tetrafluoride (TiF₄) as the precursor and the average size of the nanosheets were 1.09 μm with 64% of reactive {001} facets. Shi et al. (2014) reported the fabrication of anatase TiO₂ hollow nanosheets with the size of 550 nm having total surface area of ~17 m²g⁻¹ with the percentage of reactive facets of 65%. Similarly, many studies were carried out to get more percentage of reactive facets {001} but with large size and lower surface area (Dozzi & Sellì 2013; Gu et al. 2012; Ruso et al. 2013). F⁻ ions tend to selectively adsorb on the surface of {001} facets and as a result, it lowers the surface free energy of the reactive facets and stabilize them (Shi et al. 2014). Therefore, in order to have more specific surface area for higher interaction between reactant particles, a smaller particle size with more percentage of reactive facets is thus required. There are very few contributions were reported earlier with respect to this concern. A novel hydrothermal route is reported in this study to synthesize small sized TiO₂ nanosheets with higher percentage of reactive {001} facets using anatase TiO₂ nanomaterials as the precursor.

EXPERIMENTAL DETAILS

Synthesis of TiO₂ nanosheets Titania nanosheets (TNS) were prepared using a two-step procedure. In the first step, titania nanotubes (TNT) were synthesized from a commercially available pure anatase titania nanopowder with 99.7% purity (Sigma-Aldrich). In a typical procedure, TNTs were prepared using a hydrothermal process by mixing TiO₂ nanopowder with ethanol and NaOH solution (10 M), followed by hydrothermal treatment of the mixture at 180°C in a teflon-lined

autoclave for 24 h. After the hydrothermal reaction, the products of the reaction were washed and dried properly and denoted as TNT. Later on, for the synthesis of TNS, the prepared TNTs were mixed in an appropriate amount of ethanol and a very small amount of hydrofluoric acid (0.2 mL) (40%). The solution was then transferred to the dry teflon-lined autoclave for further hydrothermal chemical treatment at 180°C for 24 h. The obtained products were filtered and washed with deionized water and they are later dried at 80°C for 6 h.

Characterization The following characterization techniques were used for the synthesized catalyst.

Field Emission Scanning Electron Microscopy (FE-SEM)

The morphology, particle size distribution or structure of TNSs was determined by using ZEISS FE-SEM (SUPRA 55VP). A secondary electron detector (In Lens) was used to take all the SEM images. The applied accelerating voltage (EHT) was 7.00 kV with a resolution (WD) of 3.8 mm.

High Resolution Transmission Electron Microscopy (HR-TEM)

TiO₂ nanosheets samples were dispersed on a carbon film supported by a copper grid for HR-TEM observation (Model Zeiss LIBRA 200 FE) operated at 200 kV with the magnification of 80,000 and 200,000.

X-Ray Diffraction Studies (XRD)

Powder X-ray diffraction (XRD) data was analyzed using Shimadzu (Kyoto, Japan) XRD-6000 diffractometer with Cu Kα radiation (λ = 1.5418 nm) and graphite monochromator operated at 30 kV, 30 mA and 25°C. The XRD pattern was recorded in the range of 2θ = 2–80°.

Raman Spectroscopy

The Raman spectrum was recorded using Horiba Jobin Yvon HR 800 instrument with the He-Ne laser of 514.53 nm wavelength.

Accelerated Surface Area and Porosimetry (ASAP)

The pore volume and surface area of TNS were obtained by N₂ adsorption-desorption isotherm at 77 K on Micromeritics, TRISTAR II 3020 apparatus. The sample was degassed at 300°C for 240 min prior to N₂ adsorption.

UV-vis diffused reflectance spectroscopy (UV-vis DRS)

The UV-vis DRS spectra for the TNS sample and commercial TiO₂ sample were carried out using UV-vis spectrophotometer (Shimadzu UV3150 NIR). During the UV-vis diffuse reflectance experiment, BaSO₄ was used as reflectance standard.

X-ray photoelectron spectroscopy (XPS)

The XPS measurement was done in VG ESCALAB 210 electron spectrometer. The spectra were plotted using Al Kα (1253.6 eV) radiation in the constant analyser energy mode with a pass energy of 200 eV.

RESULTS AND DISCUSSION

Figure 1 shows the XRD pattern for commercial TiO_2 nanopowder, TNTs and synthesized TiO_2 nanosheets (TNS). The XRD pattern of commercial TiO_2 nanopowder (P25) shows peaks for both anatase and rutile phase as it is composed of 80% anatase and 20% rutile phase. However, XRD pattern of TNTs shows major diffraction peaks at 24.2° , 28.4° and 48.3° which are characteristic of the tubular $\text{Ti}_3\text{O}_7^{2-}$ ($\text{Na}_2\text{Ti}_3\text{O}_7/\text{H}_2\text{Ti}_3\text{O}_7$) resulted after the NaOH treatment of TiO_2 nanopowder, while Na^+ is replaced with H^+ during washing process (Lu et al. 2015; Tsai & Teng 2006; Vu et al. 2014). The XRD pattern of the TNS catalyst clearly depicts the crystalline nature as well as pure anatase phase of the TiO_2 particles (JCPDS 21-1272). The absence of diffraction peaks at $2\theta = 27$ or 31° in XRD pattern indicate that there is no rutile or brookite impurities in the pure anatase TiO_2 nanosheets structures, which is also confirmed by the literature (Gu et al. 2012). Moreover, a sharp and good intensity peak of (200) was observed indicating the growth of crystal in the direction of [100], resulting in increased side length of the crystal. On the other hand, a slightly broader diffraction peak of (004) indicates the decrease of crystal thickness in the direction of [001] (Madsen et al. 2011).

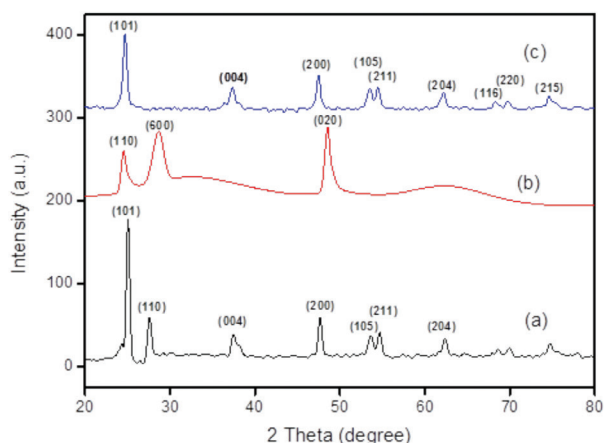


FIGURE 1. Typical XRD pattern of (a) TiO_2 (b) TNT (c) as synthesized TNS

Raman spectrum for TNS (Figure 2) is also in good agreement with XRD results. Peaks at 144 , 394 , 514 and 636 cm^{-1} confirmed the presence of titania anatase phase of crystalline TNS structure. The peaks at 144 and 636 cm^{-1} are referred as Eg peaks, which correspond to the symmetric stretching vibrations of O–Ti–O bonds in anatase TiO_2 structure. In addition, the peaks at 394 and 514 cm^{-1} represent B1g and A1g, indicating symmetric and antisymmetric bending vibrations of O–Ti–O bonds, respectively. For the anatase titania with high percentage of {001} reactive facets, the crystal surface possesses more under-coordinated Ti and O atoms, which contributes towards the increased symmetric and antisymmetric bending vibrations of O–Ti–O bonds. As

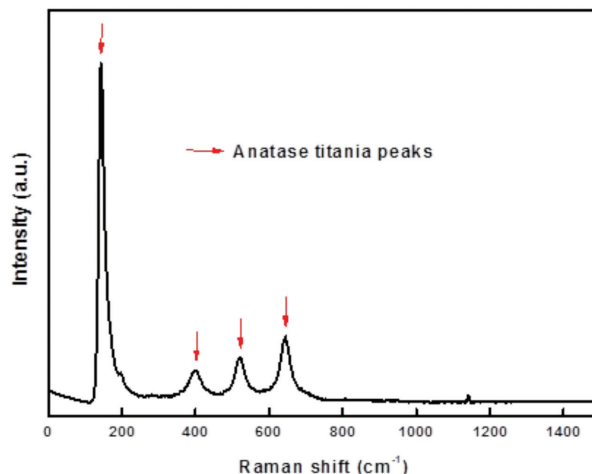


FIGURE 2. Raman spectrum of TNS

a result, prominent peaks of B1g and A1g appear in the Raman spectrum (Tian et al. 2012). Figure 3 clearly depicts the surface morphology and crystalline characteristics of commercial TiO_2 nanopowder (a), synthesized TiO_2 nanotubes (b) and synthesized TiO_2 nanosheets (c & d). The observed particle size of commercial TiO_2 , TNT and the synthesized TNS nanoparticles were in the range of 10–50 nm, 100–200 nm (width 20–50 nm) and 20–40 nm, respectively. The TEM images (Figure 3(d)) clearly indicates the lattice spacing of 0.235 nm is parallel to the top and the bottom planes, while the lattice spacing of 0.348 nm is parallel to the sides of crystalline nanosheets correspond to {001} and {101} facets, respectively. The interfacial angle between these two crystalline facets were found to be 68.3° (Figure 3(c)), which is same with the theoretical value as reported by several researchers (Dai et al. 2013; Diebold 2003; Gu et al. 2012).

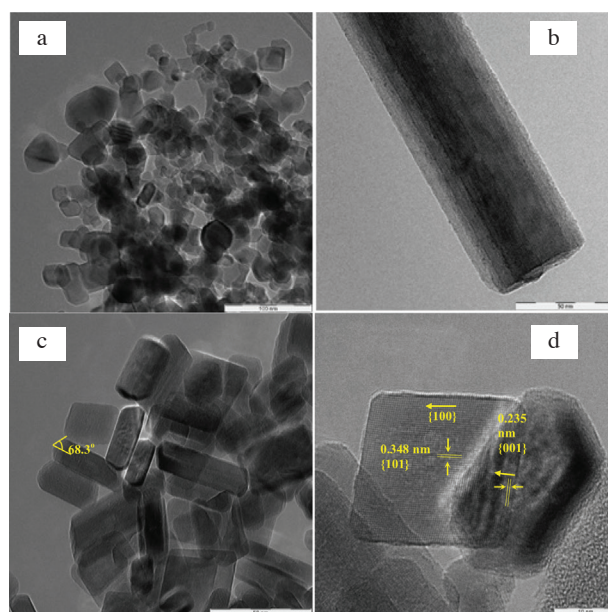


FIGURE 3. TEM images of (a) commercial TiO_2 nanopowder, (b) TNTs, (c) and (d) TNS

According to the structural information from TEM and HR-TEM results, the percentage of the exposed reactive crystal facets $\{001\}$ was about 60% of the total surface area of the crystal structure. Figure 4 illustrates the symmetries of TNS in 3D structure that helps in understanding the geometry of TNS and theoretical calculation for the determination of percentage of highly reactive $\{001\}$ crystal facet. The reason for a high percentage of reactive $\{001\}$ facets in TNS structure is due to the active participation of hydrofluoric acid (HF) during the growth of the crystal structure. Additionally, the co-adsorption of ethanol effectively strengthened the interaction of F^- ion with the surface of $\{001\}$ facet. Thus, the selective adsorption of even small amount of F^- ion on the surface of exposed $\{001\}$ facets, restricted the further growth of crystal structure along this facet and therefore, stabilizing the $\{001\}$ planes to form nanosheets structure (Dozzi & Selli 2013; Yu et al. 2010). Consequently these give a high percentage of the exposed reactive crystal facets. From the selected area electron diffraction (SAED) pattern (Figure

3(b)), it is obvious that all the diffraction rings can be indexed to the tetragonal TiO_2 phase along the $\{001\}$ zone axis. The indexed crystal planes of SAED (110), (200), (211) and (220) confirm the presence of exposed $\{001\}$ facets.

Nitrogen adsorption-desorption isotherms were measured for TNS as well as titania nanopowder and TNT for comparison, in order to determine the surface area and pore size distribution (Figure 5). The BET specific surface area of as synthesized nanosheets was found to be $73 \text{ m}^2/\text{g}$, whereas, the BET surface area for titania nanopowder and TNT were 48 and $34 \text{ m}^2/\text{g}$, respectively. The BET surface area for TNT decreases as compared to the titania nanopowder due to the growth of titania nanotube crystalline structure. On the other hand, BET surface area of TNS increases, which is due to restricted growth of TiO_2 along $[001]$ direction and smaller size of TNS.

A higher surface area is responsible for higher adsorption of reactant molecules on the surface of catalyst due to more number of active sites (Wei et al. 2013). The TNS sample showed type IV isotherm according

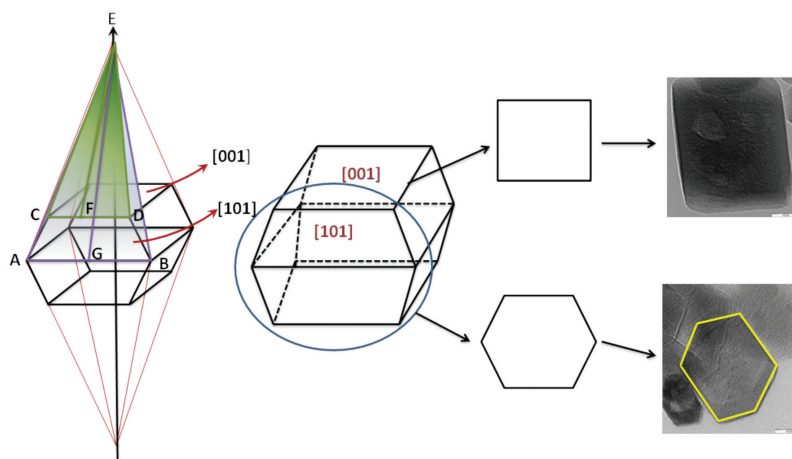


FIGURE 4. Schematic illustration of symmetries of synthesized TNS

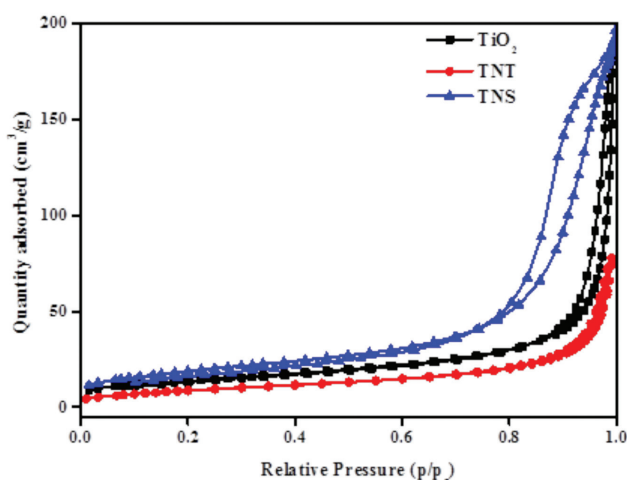


FIGURE 5. Nitrogen adsorption-desorption isotherms of commercial TiO_2 , TNT and TNS

to IUPAC classification, which represents the existence of mesoporous structure with H3 type hysteresis loop indicates the presence of slit-like pores (An et al. 2012). However, nitrogen isotherm for commercial TiO_2 shows a hysteresis loop of type H2 indicating the presence of ink-bottle like pores, with narrow necks and wider bodies. The change in the shape of hysteresis loop from H2 to H3 confirms the change in the pore structure as the TNTs transforms to TNS structure in the presence of fluoride ions. Therefore, the presence of F^- ions significantly affect the pore structure of synthesized nanosheets as explained above. The N_2 adsorption-desorption isotherm showed high absorption at high relative pressure (P/P_0) of 1.0, which represents the emergence of large mesopores (2-50 nm) (Xiang et al. 2010; Yu et al. 2010). The average pore sizes of commercial TiO_2 nanopowder, TNT and TNS, calculated using adsorption branch of the nitrogen isotherm by the BJH method are 21.8, 13.5 and 9.8 nm, respectively and the total pore volume of the catalysts are 0.268, 0.122 and $0.215 \text{ cm}^3/\text{g}$, respectively.

UV-vis diffuse reflectance spectra of TNS and commercial TiO_2 nanoparticles are compared in Figure 6 in order to understand their light absorption properties. Higher absorption of UV-vis light is related to higher catalytic activity which can be seen through UV-vis DRS results. Considerable absorption of light was recorded below 400 nm for commercial TiO_2 sample. The extrapolation of the graph for commercial TiO_2 shows the absorption edge at $\sim 390 \text{ nm}$ corresponding the band gap of 3.2 eV ($1239/\lambda$), which is due to the transition of valence electrons to conduction band (Yu et al. 2003). The commercial TiO_2 showed higher absorption in UV region and lower absorption in visible region. However, the TNS sample shows higher absorption of light in UV region as well as in visible range as compared to the commercial TiO_2 and represents a fall at $\sim 412 \text{ nm}$, yielding the band gap value of 3.0 eV representing red shift. Hence, the TNS catalyst can extend the absorption range to the visible region and narrow the band gap. Therefore, it enhances the quantum

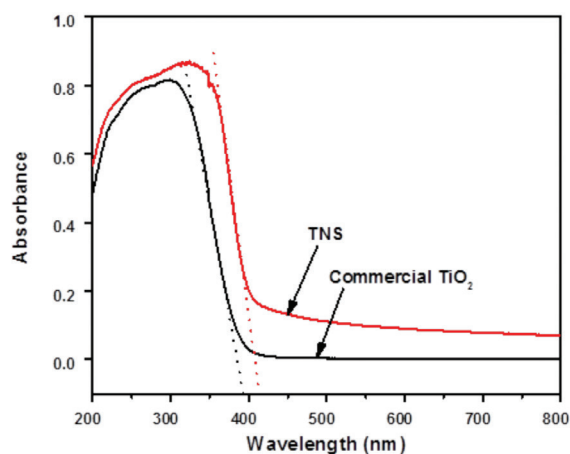


FIGURE 6. Diffused UV adsorption spectra of commercial TiO_2 and TNS

yield which corresponds to higher catalytic activity (Reddy et al. 2003).

Figure 7 depicts the XPS survey spectra of TNS nanoparticles. Sharp peak of photo electron at the binding energies of 458 eV corresponds to Ti 2p, while the peak at 531 eV corresponds to O 1s. The peak at 285 eV belongs to C 1s peak which is due to the contamination from the XPS instrument itself. However, the peak at 684.5 eV is for F 1s peak which confirms the surface fluorination of TNS structure but the amount of fluorine was found to be only 5.4%.

Based on above observations, the formation mechanism for TNS followed by the formation of TNTs is proposed as follows. During the formation of TNTs, TiO_2 undergoes crystal structure transformation in the presence of aqueous solution of NaOH. Anatase TiO_2 crystallite experiences exfoliation in the form of trititanate $(\text{Ti}_3\text{O}_7)^{2-}$ sheets caused by the reaction between NaOH and TiO_2 (An'Amr et al. 2014; Noor et al. 2013). The nanosheets grow with an increasing tendency of curling due to its unstable and high surface energy structure, leading to the formation of nanotubes. Where the hydrogen-deficiency on the surface of $(\text{Ti}_3\text{O}_7)^{2-}$ plates can provide the driving force (surface tension) for the peeling-off of $(\text{Ti}_3\text{O}_7)^{2-}$ plates and therefore resulting in the layers bent to form tube morphology and thus lowers the system energy (Ou & Lo 2007). The Na^+ ions that were excessively intercalated between the spaces of anatase TiO_2 crystals are washed off with HCl and most of the Na^+ ions are replaced with H^+ ions (Chu et al. 2016; Vaenas et al. 2015). However, these TNTs when undergo 2nd step of hydrothermal treatment in the presence of HF and ethanol, it causes the tube structure of TNTs to re-open into sheet like structure. The anatase TiO_2 in TNTs possess both H- and O-terminated surfaces with high surface energy thus, restricts the formation of large anatase sheets. Fluorine being low bonding energy element and having strong bonding ability with Ti can provide an effective mean to stabilize the high energy surface (Dozzi & Selli 2013; Zhang et al. 2015). Among other anatase crystalline facets, {001} surfaces are favourably fluorinated and hence energetically stabilized as compared to {101} surfaces (Wen et al. 2015). Consequently, preventing the anatase TiO_2 sheets from rolling back. Moreover, addition of ethanol plays the role of synergistic capping agent and reaction medium along with HF. It has also been confirmed through various theoretical and experimental evidences that lower alcohols act as protecting agents. They dissociates heterolytically in acidic mediums to give alkoxy groups ($\text{CH}_3\text{CH}_2\text{O}^-$), which bind to under-coordinated Ti^{4+} cations on the surface of {001} and {101} facets (Yang et al. 2009). However, preferential adsorption occurs on {001} facets due to higher density of 5-fold coordinated Ti on {001} facets which results in restricted growth of crystal in [001] direction.

On the other hand, direct use of TiO_2 (instead of TNT as precursor) for the formation of TNS will lead to untransformed crystal structures that will otherwise occur in the presence of NaOH. Therefore, it is believed that

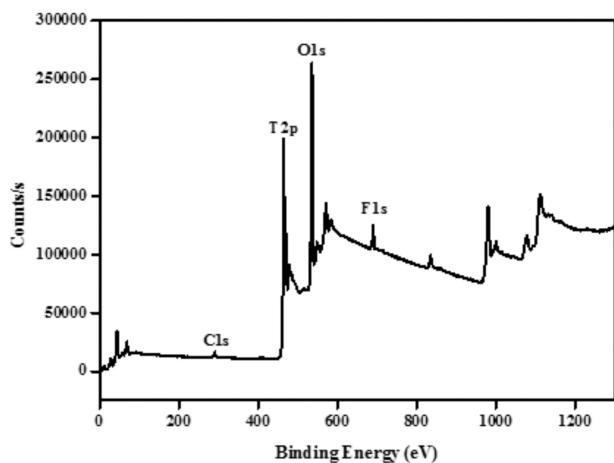


FIGURE 7. XPS survey spectra of TNS

without NaOH treatment, which is actually responsible for the transformation of anatase TiO_2 particles into sheet like structure, there would be no stabilized $\{001\}$ exposed crystal facets. Resultantly, TNS without NaOH treatment are expected to show low catalytic activity due to absence of $\{001\}$ exposed crystal facets. Hence, the remarkable features of solvothermally synthesized TNS via two step procedure make it suitable for various catalytic applications.

CONCLUSION

The TiO_2 nanosheet-like structures were successfully synthesized by a simple solvothermal chemical route using hydrofluoric acid and ethanol as capping and stabilizing agents. These synthesized nanosheets have small size in the range of 20-40 nm with high surface area of 73 m^2/g . In addition, the majority of this specific surface area is composed of highly reactive exposed $\{001\}$ facets (60%). The synthesized nanocatalyst is expected to have high catalytic activity due to its small size, high surface area and high percentage of exposed highly reactive $\{001\}$ facets. The present work motivates us to further utilize the synthesized TiO_2 nanosheets in the field of biofuel production, due to its promising characteristics as nanocatalyst.

ACKNOWLEDGEMENTS

The authors highly appreciate and regard the financial support from Universiti Teknologi PETRONAS.

REFERENCES

An'Amt, M.N., Huang, N.M., Radiman, S., Lim, H.N. & Muhamad, M.R. 2014. Triethanolamine-solution for rapid hydrothermal synthesis of titanate nanotubes. *Sains Malaysiana* 43(1): 137-144.

An, T., Chen, J., Nie, X., Li, G., Zhang, H., Liu, X. & Zhao, H. 2012. Synthesis of carbon nanotube-anatase TiO_2 sub-micrometer-sized sphere composite photocatalyst for

synergistic degradation of gaseous styrene. *ACS Applied Materials & Interfaces* 4(11): 5988-5996.

Biyoghe Bi Ndong, L., Ibondou, M.P., Gu, X., Lu, S., Qiu, Z., Sui, Q. & Mbadinga, S.M. 2014. Enhanced photocatalytic activity of TiO_2 nanosheets by doping with Cu for chlorinated solvent pollutants degradation. *Industrial and Engineering Chemistry Research* 53(4): 1368-1376.

Cai, J., Huang, Z., Lv, K., Sun, J. & Deng, K. 2014. Ti powder-assisted synthesis of Ti^{3+} self-doped TiO_2 nanosheets with enhanced visible-light photoactivity. *RSC Advances* 4(38): 19588-19593.

Cao, X., Tian, G., Chen, Y., Zhou, J., Zhou, W., Tian, C. & Fu, H. 2014. Hierarchical composites of TiO_2 nanowire arrays on reduced graphene oxide nanosheets with enhanced photocatalytic hydrogen evolution performance. *Journal of Materials Chemistry A* 2(12): 4366-4374.

Chang, J.B., Liu, C.H., Liu, J., Zhou, Y.Y., Gao, X. & Wang, S.D. 2015. Green-chemistry compatible approach to TiO_2 -supported PdAu bimetallic nanoparticles for solvent-free 1-phenylethanol oxidation under mild conditions. *Nano-Micro Letters* 7(3): 307-315.

Chao, C., Ren, Z., Yin, S., Xu, G., Gong, S., Yang, X., Li, X., Shen, G. & Han, G. 2014. Dissolution/recrystallization growth of titanate nanostructures by amorphous precursor. *Advanced Powder Technology* 25(2): 745-751.

Chen, C., Hu, X., Wang, Z., Xiong, X., Hu, P., Liu, Y. & Huang, Y. 2014. Controllable growth of TiO_2 -B nanosheet arrays on carbon nanotubes as a high-rate anode material for lithium-ion batteries. *Carbon* 69: 302-310.

Chu, M., Tang, Y., Rong, N., Cui, X., Liu, F., Li, Y., Zhang, C., Xiao, P. & Zhang, Y. 2016. Hydrothermal synthesis, and tailoring the growth of Ti-supported TiO_2 nanotubes with thick tube walls. *Materials & Design* 97: 257-267.

Dai, H., Zhou, Y., Chen, L., Guo, B., Li, A., Liu, J., Yu, T. & Zou, Z. 2013. Porous ZnO nanosheet arrays constructed on weaved metal wire for flexible dye-sensitized solar cells. *Nanoscale* 5(11): 5102-5108.

Deng, L.J., Gu, Y.Z., Xu, W.X. & Ma, Z.Y. 2014. Preparation of TiO_2 nanocrystals/graphene composite and its photocatalytic performance. *Chinese Journal of Chemical Physics* 27(3): 321-326.

Diebold, U. 2003. The surface science of titanium dioxide. *Surface Science Reports* 48(5-8): 53-229.

Dozzi, M.V. & Selli, E. 2013. Specific facets-dominated anatase TiO_2 : Fluorine-mediated synthesis and photoactivity. *Catalysts* 3(2): 455-485.

Gu, L., Wang, J., Cheng, H., Du, Y. & Han, X. 2012. Synthesis of nano-sized anatase TiO_2 with reactive $\{001\}$ facets using lamellar protonated titanate as precursor. *Chemical Communications* 48(55): 6978-6980.

Liu, S., Yu, J. & Jaroniec, M. 2011. Anatase TiO_2 with dominant high-energy $\{001\}$ facets: Synthesis, properties, and applications. *Chemistry of Materials* 23(18): 4085-4093.

Lu, H., Wang, Y., Wang, Y., Liang, W. & Yao, J. 2015. Adjusting phase transition of titania-based nanotubes via hydrothermal and post treatment. *RSC Advances* 5(109): 89777-89782.

Madiha Yasir, S.C., Nurlidia Mansor, Norani Muti Mohamed & Yoshimitsu Uemura. 2014. Upgrading of pyrolysis bio-oil to fuel over supported nanomaterials - A review. *Applied Mechanics and Materials* 625: 357-360.

Madsen, A.T., Ahmed, E.H., Christensen, C.H., Fehrmann, R. & Riisager, A. 2011. Hydrodeoxygenation of waste fat for diesel

- production: Study on model feed with Pt/alumina catalyst. *Fuel* 90(11): 3433-3438.
- Noor, A.M., Ming, H., Ngee, L., Radiman, S., Rahim, S., Ahmad, S.I., Shamsudin, S.A., Yarmo, M.A. & Sajab, M.S. 2013. Synthesis and morphology control of TiO₂ nano structures via hydrothermal method for applications as electrodes in dye-sensitized solar cells. *Sains Malaysiana* 42(7): 967-974.
- Ou, H.H. & Lo, S.L. 2007. Review of titania nanotubes synthesized via the hydrothermal treatment: Fabrication, modification, and application. *Separation and Purification Technology* 58(1): 179-191.
- Reddy, K.M., Manorama, S.V. & Reddy, A.R. 2003. Bandgap studies on anatase titanium dioxide nanoparticles. *Materials Chemistry and Physics* 78(1): 239-245.
- Ruso, J.M., Verdinelli, V., Hassan, N., Pironi, O. & Messina, P.V. 2013. Enhancing CaP biomimetic growth on TiO₂ cuboids nanoparticles via highly reactive facets. *Langmuir* 29(7): 2350-2358.
- Shi, Q., Li, Y., Zhan, E., Ta, N. & Shen, W. 2014. Anatase TiO₂ hollow nanosheets: Dual roles of F⁻ formation mechanism, and thermal stability. *CrystEngComm* 16(16): 3431-3437.
- Tian, F., Zhang, Y., Zhang, J. & Pan, C. 2012. Raman spectroscopy: A new approach to measure the percentage of anatase TiO₂ exposed (001) facets. *The Journal of Physical Chemistry C* 116(13): 7515-7519.
- Tsai, C.C. & Teng, H. 2006. Structural features of nanotubes synthesized from NaOH treatment on TiO₂ with different post-treatments. *Chemistry of Materials* 18(2): 367-373.
- Vaenas, N., Stergiopoulos, T. & Falaras, P. 2015. Titania nanotubes for solar cell applications. In *Electrochemically Engineered Nanoporous Materials: Methods, Properties & Application*, edited by Losic, D. & Santos, A. New York: Springer pp. 289-306.
- Vu, T.H.T., Au, H.T., Tran, L.T., Nguyen, T.M.T., Tran, T.T.T., Pham, M.T., Do, M.H. & Nguyen, D.L. 2014. Synthesis of titanium dioxide nanotubes via one-step dynamic hydrothermal process. *Journal of Materials Science* 49(16): 5617-5625.
- Wei, X., Zhu, G., Fang, J. & Chen, J. 2013. Synthesis, characterization, and photocatalysis of well-dispersible phase-pure anatase TiO₂ nanoparticles. *International Journal of Photoenergy* 2013: Article ID. 726872.
- Wen, M., Liu, P., Xiao, S., Mori, K., Kuwahara, Y., Yamashita, H., Li, H. & Zhang, D. 2015. Uniform anatase single-crystal cubes with high thermal stability fully enclosed by active {010} and {001} facets. *RSC Advances* 5(15): 11029-11035.
- Xiang, Q., Lv, K. & Yu, J. 2010. Pivotal role of fluorine in enhanced photocatalytic activity of anatase TiO₂ nanosheets with dominant (001) facets for the photocatalytic degradation of acetone in air. *Applied Catalysis B: Environmental* 96(3-4): 557-564.
- Xiaowei, L., Yanqiu, J., Wenjing, C., Yudong, L., Xianzhu, X. & Kaifeng, L. 2015. Mesoporous TiO₂/carbon beads: One-pot preparation and their application in visible-light-induced photodegradation. *Nano-Micro Letters* 7(3): 243-254.
- Xinwen, H. & Zongjian, L. 2013. Synthesis and growth mechanism of net-like titanate nanowire films via low-temperature and low-alkali-concentration route. *Nano-Micro Letters* 5(2): 93-100.
- Yang, H.G., Liu, G., Qiao, S.Z., Sun, C.H., Jin, Y.G., Smith, S.C., Zou, J., Cheng, H.M. & Lu, G.Q. 2009. Solvothermal synthesis and photoreactivity of anatase TiO₂ nanosheets with dominant {001} facets. *Journal of the American Chemical Society* 131(11): 4078-4083.
- Yifan, C., Jiahua, N., Hongliu, W., Ruopeng, Z., Changli, Z., Wenzhi, C., Feiqing, Z., Shaoliang, Z. & Xiaonong, Z. 2015. Study of cell behaviors on anodized TiO₂ nanotube arrays with coexisting multi-size diameters. *Nano-Micro Letters* 7: 215-225.
- Yu, J., Fan, J. & Lv, K. 2010. Anatase TiO₂ nanosheets with exposed (001) facets: Improved photoelectric conversion efficiency in dye-sensitized solar cells. *Nanoscale* 2(10): 2144-2149.
- Yu, J.C., Zhang, L., Zheng, Z. & Zhao, J. 2003. Synthesis and characterization of phosphated mesoporous titanium dioxide with high photocatalytic activity. *Chemistry of Materials* 15(11): 2280-2286.
- Zhang, B., Wei, F., Wu, Q., Piao, L., Liu, M. & Jin, Z. 2015. Formation and evolution of the high-surface-energy facets of anatase TiO₂. *The Journal of Physical Chemistry C* 119(11): 6094-6100.

Madiha Yasir, M. Tazli Azizan* & Mariam Ameen
 Chemical Engineering Department
 Universiti Teknologi PETRONAS
 31750 Tronoh, Perak Darul Ridzuan
 Malaysia

Anita Ramli
 Department of Fundamental and Applied Sciences
 Universiti Teknologi PETRONAS
 32610 Bandar Seri Iskandar, Perak Darul Ridzuan
 Malaysia

M. Tazli Azizan* & Anita Ramli
 Center for Biofuel and Biochemical Research (CBBR)
 Universiti Teknologi PETRONAS
 31750 Tronoh, Perak Darul Ridzuan
 Malaysia

*Corresponding author; email: tazliazizan@utp.edu.my

Received: 18 December 2015

Accepted: 5 September 2016